

Drift-Alfven instabilities of a finite beta plasma sheared flow along a magnetic field with inhomogeneous ion temperature

V. V. Mikhailenko,^{1,2, a)} V. S. Mikhailenko,^{1, b)} and Hae June Lee^{3, c)}

¹⁾ *Plasma Research Center, Pusan National University, Busan 46241, South Korea.*

²⁾ *BK21 Plus Information Technology, Pusan National University, Busan 46241, South Korea.*

³⁾ *Department of Electrical Engineering, Pusan National University, Busan 46241, South Korea.*

(Dated: 9 November 2021)

The drift-Alfven instabilities in the magnetic field aligned (parallel) sheared flow of a finite beta ($1 > \beta > m_e/m_i$) plasma with comparable inhomogeneous ion temperature and homogeneous electron temperature are examined. The development of instabilities are quantitatively discussed on the basis of numerical solution of a set of equations for the electrostatic and electromagnetic potentials. It is found that the accounting for the electromagnetic ion kinetic response, which has been ignored usually in existing discussions of the drift-Alfven instabilities of a steady plasma, reveals new drift-Alfven instability driven by the coupled action of the ion temperature gradient, the flow velocity shear, and the ion Landau damping. The excited unstable waves have the phase velocities along the magnetic field comparable with the ion thermal velocity, and the growth rate comparable with the frequency.

I. INTRODUCTION

The understanding of instabilities driven by a shear in the velocity of a plasma flows is of considerable interest to research in magnetic fusion plasmas, where inhomogeneous flows and currents along and across magnetic field are ubiquitous. It is well known, that the magnetic field aligned plasma shear flows, which are observed in the edge layers of tokamak plasmas¹⁻⁵ are the additional sources of free energy for the electrostatic and electromagnetic instabilities development. The majority of analysis of these instabilities have been restricted to the case of cold ions with ion temperature T_i much less than the electron temperature T_e . In this case the analysis may be simplified by considering the ions in the fluid limit which is valid only for the perturbations having the phase velocity along the magnetic field that greatly exceeds the thermal velocity of the ions v_{Ti} . For the tokamak plasma, the ionosphere and the solar wind plasmas the case of warm ions having the temperature comparable with or even exceeding the electron temperature is more relevant.

In parallel shear flows with hot ions, $T_i \gtrsim T_e$, the ion kinetic effects play the decisive role in the development the instabilities of the parallel shear flows. In particular, such plasma is prone to the excitation of the shear-flow driving instabilities^{6,7}. It was obtained⁷, that in plasma with inhomogeneous density the ion kinetic drift-Alfven (DA) instability develops from the coupled action of the parallel-flow shear and ion Landau damping. The growth rate of this instability is of the order of the frequency, the phase velocity of perturbations along the magnetic field

is comparable with ion thermal velocity. The electromagnetic response of the ions for this instability is comparable with the electromagnetic response of the electrons.

It was found in Ref.⁶, that the electrostatic instability exists by virtue of the coupled action of parallel velocity shear, ion Landau damping and a ion temperature gradient, which reinforce each other in the development of the ion kinetic instability. In this paper we undertake the investigation of the electromagnetic counterpart of that instability: the DA instability of the parallel shear flow with inhomogeneous ion temperature. In Section II, we present the basic linear equations that govern the stability properties of the parallel shear flows with inhomogeneous flow density and inhomogeneous ion temperature. In Section III, we present the numerical solution and discussion of the detected electromagnetic DA instabilities with special emphasis on the thermal and electromagnetic effects of ions on the stability properties of the parallel shear flows. Conclusions are given in Section IV.

II. BASIC EQUATIONS

The tokamak plasma is, as a rule, a low β plasma, with $1 \gg \beta \gg m_e/m_i$. It is well known, that such a plasma is unstable against the development of the electromagnetic DA instabilities⁸. These instabilities are governed by the Vlasov equations for electrons and ions and the Poisson equation and Ampere's law for the electrostatic potential Φ and along magnetic field component A_z of the electromagnetic potential. For the inhomogeneous, magnetic-field-aligned, single-ion-species, collisionless plasma flow with velocity $\mathbf{V}_0(X_\alpha) \parallel B_0 \mathbf{e}_z$, the Vlasov equation for the perturbation $f_\alpha = F_\alpha - F_{0\alpha}$ of the distribution function F_α with equilibrium function $F_{0\alpha}$ in guiding center coordinates in slab geometry, $X_\alpha = x + \frac{v_\perp}{\omega_{c\alpha}} \sin \phi$, $Y_\alpha = y - \frac{v_\perp}{\omega_{c\alpha}} \cos \phi$, where x and y are coordinates of the

^{a)} E-mail: vladimir@pusan.ac.kr

^{b)} E-mail: vsmikhailenko@pusan.ac.kr

^{c)} E-mail: haejune@pusan.ac.kr

particle position, $\omega_{c\alpha}$ is the cyclotron frequency, has a form

$$\begin{aligned} & \frac{\partial f_\alpha}{\partial t} - \omega_{c\alpha} \frac{\partial f_\alpha}{\partial \phi} + v_z \frac{\partial f_\alpha}{\partial z} \\ &= \frac{e}{m_\alpha} \left[\frac{1}{\omega_{c\alpha}} \left(\frac{\partial \Phi}{\partial Y} - \frac{v_z}{c} \frac{\partial A_\parallel}{\partial Y} \right) \frac{\partial F_{0\alpha}}{\partial X} \right. \\ & \quad \left. - \frac{\omega_{c\alpha}}{v_\perp} \left(\frac{\partial \Phi}{\partial \phi} - \frac{v_z}{c} \frac{\partial A_\parallel}{\partial \phi} \right) \frac{\partial F_{0\alpha}}{\partial v_\perp} \right] \\ & + \left(\frac{\partial \Phi}{\partial z} + \frac{1}{c} \frac{\partial A_\parallel}{\partial t} - \frac{\omega_{c\alpha}}{c} \frac{\partial A_\parallel}{\partial \phi} \right) \frac{\partial F_{0\alpha}}{\partial v_z} \Big], \quad (1) \end{aligned}$$

The perturbed electrostatic potential Φ is determined by the Poisson equation

$$\Delta \Phi(\mathbf{r}, t) = -4\pi \sum_{\alpha=i,e} e_\alpha \int f_\alpha(\mathbf{v}, \mathbf{r}, t) d\mathbf{v}_\alpha. \quad (2)$$

and perturbed electromagnetic potential A_\parallel is determined by the Ampere's law

$$\Delta A_\parallel(\mathbf{r}, t) = -\frac{4\pi}{c} \sum_{\alpha=i,e} e_\alpha \int v_z f_\alpha(\mathbf{v}, \mathbf{r}, t) d\mathbf{v}_\alpha. \quad (3)$$

In what follows, $F_{0\alpha}$ is considered as the shifted Maxwellian distribution function for electrons and ions ($\alpha = i, e$)

$$F_{0\alpha} = \frac{n_{0\alpha}(X_\alpha)}{(2\pi v_{T\alpha}^2)^{3/2}} \exp \left[-\frac{v_\perp^2}{2v_{T\alpha}^2} - \frac{(v_z - V_0(X_\alpha))^2}{2v_{T\alpha}^2} \right] \quad (4)$$

assuming the inhomogeneity direction of the density and temperature of the sheared-flow species is along coordinate X_α , $v_{T\alpha} = (T_\alpha(X_\alpha)/m_\alpha)^{1/2}$ is the thermal velocity. The flow velocity of ions \mathbf{V}_0 is assumed to be equal to that of the electrons. We consider here the idealized inhomogeneous-flow case of homogeneous parallel-velocity shear, i.e. $V_0(X_\alpha) = V_{00} + V'_0 X_\alpha$, where V_{00} is the spatially homogeneous part of the flow velocity, and $V'_0 = \text{const}$. In order to simplify the problem, a velocity \mathbf{v} usually transforms from the laboratory to a convecting frame of reference, $\mathbf{v} = \hat{\mathbf{v}} + V_0(X_\alpha)\mathbf{e}_z$, where any spatially homogeneous part of flow velocity is eliminated from the problem by a simple Galilean transformation. The solution of the system (1)-(3) in the convective set of reference is of the modal form during a long time until $V'_0 t \lesssim k_x/k_z$. Until that time, the solution to Fourier transformed system (1)-(3) in the local approximation, for which $k_x L_n \gg 1$, where $L_n = [d \ln n_0(X)/dx]^{-1}$, is given by the equations

$$\begin{aligned} \Phi(\mathbf{k}, \omega) & \left[k^2 \lambda_{Di}^2 + \sum_{n=-\infty}^{\infty} A_{ni} \left[1 + i\sqrt{\pi} W(z_{ni}) \right] \right. \\ & \quad \left. \times \left(z_{0i} - \chi_i \left(1 - \frac{1}{2} \eta_i \right) \right) \right] \\ & - S_i \sum_{n=-\infty}^{\infty} A_{ni} \left(1 + i\sqrt{\pi} z_{ni} W(z_{ni}) \right) \end{aligned}$$

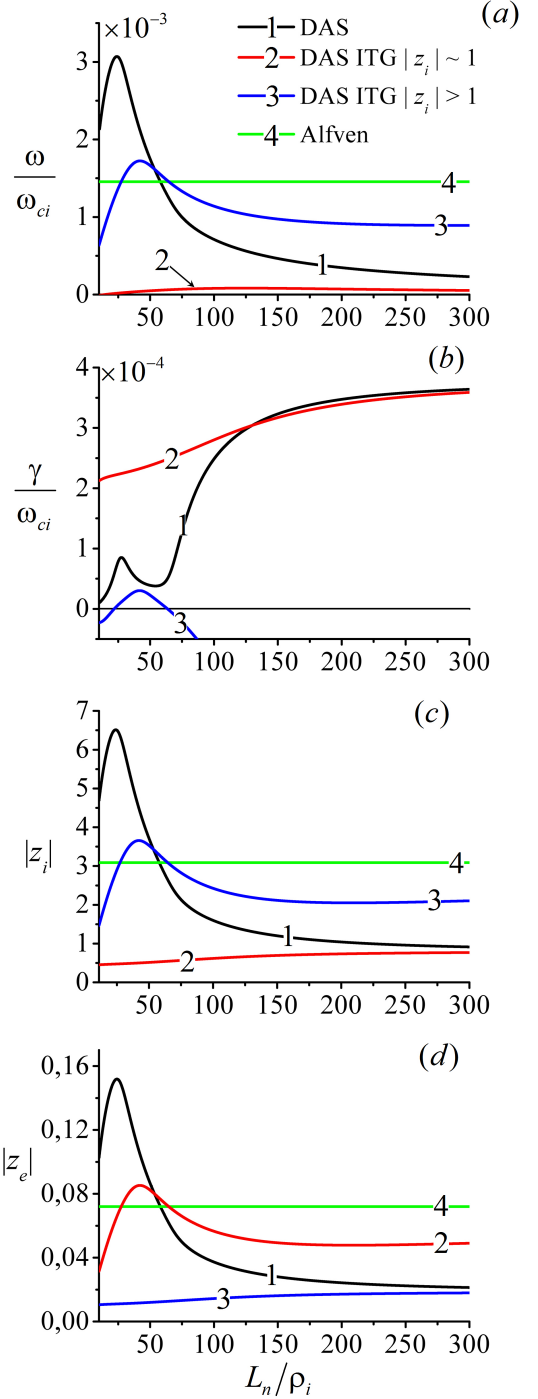


FIG. 1. The normalized frequency ω/ω_{ci} (panel (a)), the normalized growth rate γ/ω_{ci} (panel (b)), $|z_i|$ (panel (c)) and $|z_e|$ (panel (d)) versus L_n/ρ_i for $\eta_i = 3$, $k_y \rho_i = 0.1$, $T_i/T_e = 1$, $(V'_0/\omega_{ci})^{-1} = 70$, $(k_z \rho_i)^{-1} = 3000$.

$$- \sum_{n=-\infty}^{\infty} \chi_i \eta_i z_{ni} A_{ni} \left(1 + i\sqrt{\pi} z_{ni} W(z_{ni}) \right)$$

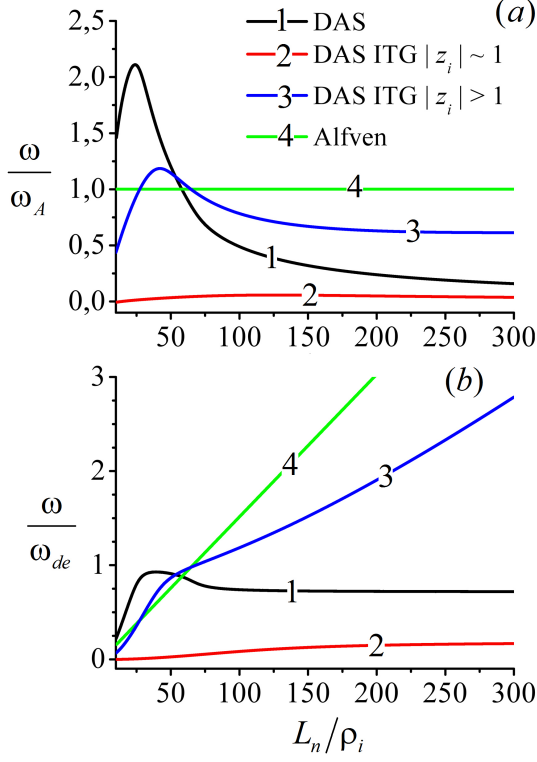


FIG. 2. The normalized frequencies ω/ω_A (panel (a)) and ω/ω_{de} (panel (b)) versus L_n/ρ_i for $\eta_i = 3$, $k_y\rho_i = 0.1$, $T_i/T_e = 1$, $(V'_0/\omega_{ci})^{-1} = 70$, $(k_z\rho_i)^{-1} = 3000$.

$$\begin{aligned}
& + i\sqrt{\pi} \sum_{n=-\infty}^{\infty} \chi_i \eta_i W(z_{ni}) k_{\perp}^2 \rho_i^2 (A_{ni} + \hat{A}_{ni}) \\
& + \tau \sum_{n=-\infty}^{\infty} A_{ne} \left(1 + i\sqrt{\pi} (z_{0e} - \chi_e) W(z_{ne}) \right) \\
& - A_{\parallel}(\mathbf{k}, \omega) \left\{ \sum_{n=-\infty}^{\infty} A_{ni} \left(z_{0i} - \chi_i \left(1 - \frac{1}{2} \eta_i \right) \right) \right. \\
& \quad \times \left(1 + i\sqrt{\pi} z_{ni} W(z_{ni}) \right) \\
& \quad \left. - S_i \sum_{n=-\infty}^{\infty} A_{ni} z_{ni} \left(1 + i\sqrt{\pi} z_{ni} W(z_{ni}) \right) \right. \quad (5) \\
& - \sum_{n=-\infty}^{\infty} \chi_i \eta_i z_{ni} A_{ni} \left[\frac{1}{2} + z_{ni}^2 \left(1 + i\sqrt{\pi} z_{ni} W(z_{ni}) \right) \right] \\
& + \sum_{n=-\infty}^{\infty} \chi_i \eta_i \left(1 + i\sqrt{\pi} z_{ni} W(z_{ni}) \right) k_{\perp}^2 \rho_i^2 (A_{ni} + \hat{A}_{ni}) \\
& \left. + \tau \frac{v_{Te}}{v_{Ti}} \sum_{n=-\infty}^{\infty} A_{ne} (z_{0e} - \chi_e) \left(1 + i\sqrt{\pi} z_{ne} W(z_{ne}) \right) \right\} = 0
\end{aligned}$$

and

$$\Phi(\mathbf{k}, \omega) \left[\sum_{n=-\infty}^{\infty} A_{ni} \left(z_{0i} - \chi_i \left(1 - \frac{1}{2} \eta_i \right) \right) \right.$$

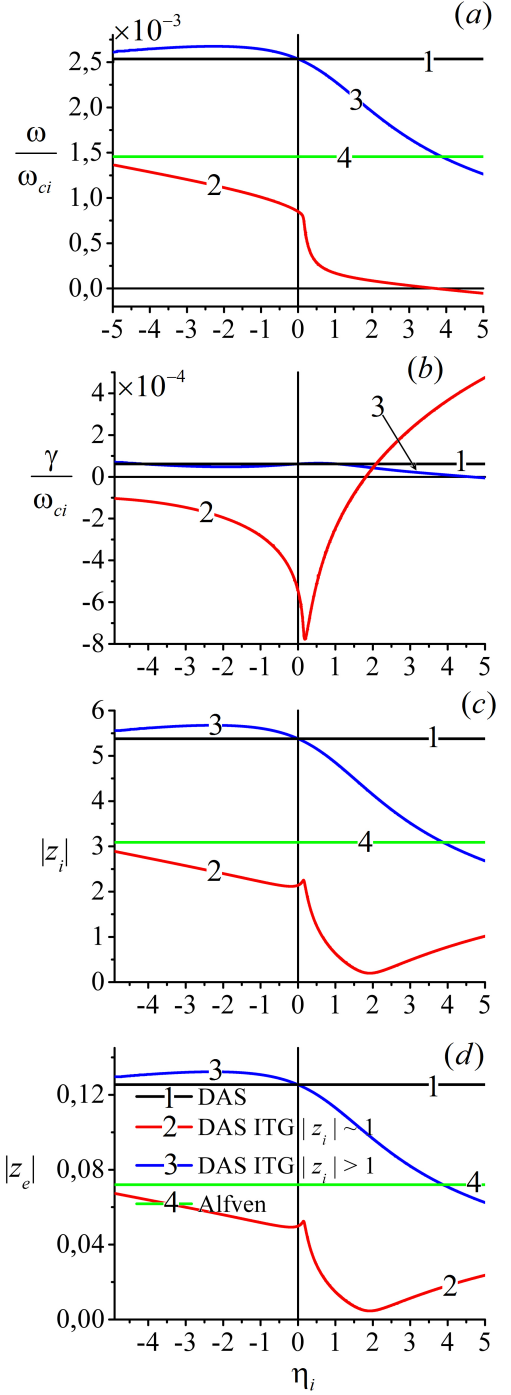


FIG. 3. The normalized frequency ω/ω_{ci} (panel (a)), the normalized growth rate γ/ω_{ci} (panel (b)), $|z_i|$ (panel (c)) and $|z_e|$ (panel (d)) versus η_i for $L_n/\rho_i = 35$, $k_y\rho_i = 0.1$, $T_i/T_e = 1$, $(V'_0/\omega_{ci})^{-1} = 70$, $(k_z\rho_i)^{-1} = 3000$.

$$\begin{aligned}
& \times \left(1 + i\sqrt{\pi} z_{ni} W(z_{ni}) \right) \\
& - S_i \sum_{n=-\infty}^{\infty} A_{ni} z_{ni} \left(1 + i\sqrt{\pi} z_{ni} W(z_{ni}) \right)
\end{aligned}$$

$$\begin{aligned}
& - \sum_{n=-\infty}^{\infty} \chi_i \eta_i z_{ni} A_{ni} \left[\frac{1}{2} + z_{ni}^2 \left(1 + i\sqrt{\pi} z_{ni} W(z_{ni}) \right) \right] \\
& + \sum_{n=-\infty}^{\infty} \chi_i \eta_i \left(1 + i\sqrt{\pi} z_{ni} W(z_{ni}) \right) k_{\perp}^2 \rho_i^2 \left(A_{ni} + \hat{A}_{ni} \right) \\
& + \tau \frac{v_{Te}}{v_{Ti}} \sum_{n=-\infty}^{\infty} A_{ne} (z_{0e} - \chi_e) \left(1 + i\sqrt{\pi} z_{ne} W(z_{ne}) \right) \\
& + A_{\parallel}(\mathbf{k}, \omega) \left\{ \frac{k_{\perp}^2 \rho_i}{2\beta} - \sum_{n=-\infty}^{\infty} \left(z_{0i} - \chi_i \left(1 - \frac{1}{2} \eta_i \right) \right) \right. \\
& \quad \times A_{ni} z_{ni} \left(1 + i\sqrt{\pi} z_{ni} W(z_{ni}) \right) \quad (6) \\
& \quad + S_i \sum_{n=-\infty}^{\infty} A_{ni} \left[\frac{1}{2} + z_{ni}^2 \left(1 + i\sqrt{\pi} z_{ni} W(z_{ni}) \right) \right] \\
& \quad + \sum_{n=-\infty}^{\infty} \chi_i \eta_i z_{ni} A_{ni} \left[\frac{1}{2} + z_{ni}^2 \left(1 + i\sqrt{\pi} z_{ni} W(z_{ni}) \right) \right] \\
& \quad - \sum_{n=-\infty}^{\infty} \chi_i \eta_i z_{ni} k_{\perp}^2 \rho_i^2 \left(A_{ni} + \hat{A}_{ni} \right) \\
& \quad \quad \times \left(1 + i\sqrt{\pi} z_{ni} W(z_{ni}) \right) \\
& \quad - \tau \frac{v_{Te}^2}{v_{Ti}^2} \sum_{n=-\infty}^{\infty} A_{ne} (z_{0e} - \chi_e) \\
& \quad \left. \times z_{ne} \left(1 + i\sqrt{\pi} z_{ne} W(z_{ne}) \right) \right\} = 0.
\end{aligned}$$

In Eqs. (5), (6) λ_{Di} is the ion Debye length, ω_{ci} is the ion cyclotron frequency, $\rho_i = v_{Ti}/\omega_{ci}$ is the ion thermal Larmor radius, $A_{ni,e} = I_n(k_{\perp}^2 \rho_{i,e}^2) e^{-k_{\perp}^2 \rho_{i,e}^2}$, $\hat{A}_{ni} = e^{-k_{\perp}^2 \rho_i^2} I_n'(k_{\perp}^2 \rho_i^2)$, I_n is the modified Bessel function of order n , $z_{ni,e} = (\omega - n\omega_{ci,e})/\sqrt{2}k_z v_{Ti,e}$, $z_{0i,e} = \omega/\sqrt{2}k_z v_{Ti,e} = z_{i,e}$, $W(z) = e^{-z^2} \left(1 + \frac{2i}{\sqrt{\pi}} \int_0^z e^{t^2} dt \right)$ is the complex error function, $\tau = T_i/T_e$, $S_i = k_y V_0'/k_z \omega_{ci}$, $v_{di,e} = (cT_{i,e}/eB_0) (d \ln n_i/dx)$, $v_{di,e}$ is ion, electron diamagnetic velocity, $\eta_i = d \ln T_i/d \ln n_i$, $\chi_{i,e} = k_y v_{di,e}/\sqrt{2}k_z v_{Ti,e}$. The principal difference of Eq. (6) from the similar equation obtained early (see, for example Ref.⁵ and the references therein) consists in the accounting for the perturbed ion current, as well as the electron current. We do not assume here, that the phase velocity of the perturbations is much above the ion thermal velocity. In the case $T_i \sim T_e$ and $|z_{0i}| \sim 1$ the electron and ion responses in Eq. (6) are of the same order.

We consider low frequency electromagnetic modes with frequency ω much less than the ion cyclotron frequency ω_{ci} in the limit $|\omega| \lesssim k_z v_{Te}$ as is appropriate for the velocity shear and the temperature gradient instabilities. For these conditions, the general dispersion equation that accounts for the parallel-flow shear and inhomogeneous profiles of ion density and ion temperature and accounts for the effects of thermal motion of ions, both along and

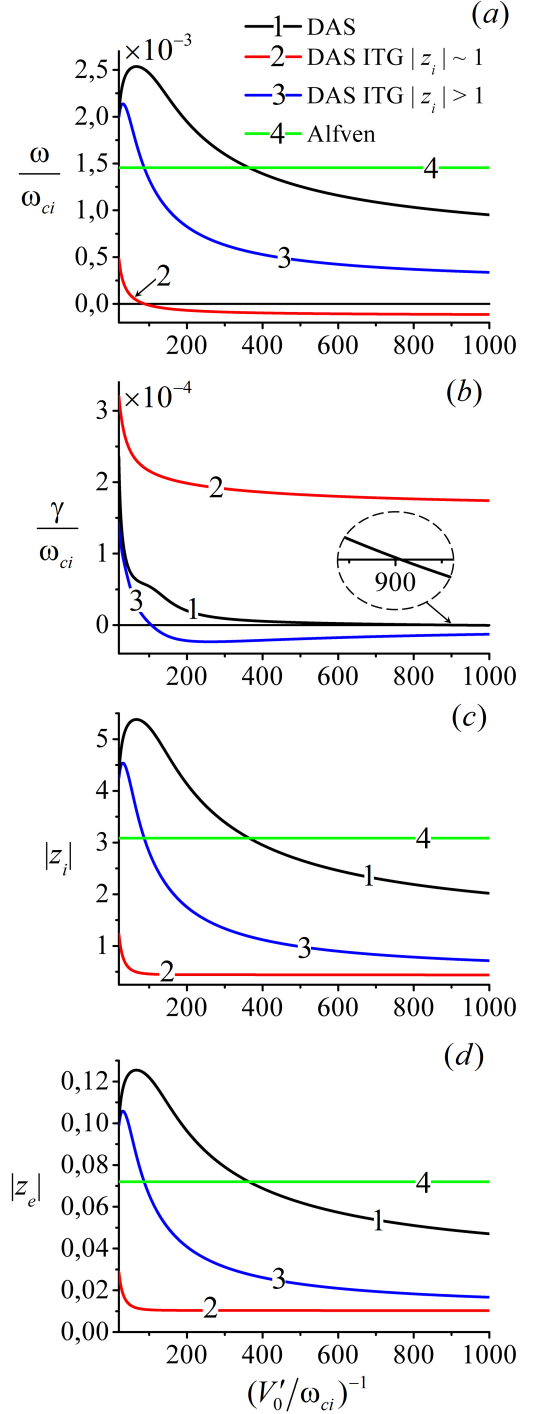


FIG. 4. The normalized frequency ω/ω_{ci} (panel (a)), the normalized growth rate γ/ω_{ci} (panel (b)), $|z_i|$ (panel (c)) and $|z_e|$ (panel (d)) versus $(V_0'/\omega_{ci})^{-1}$ for $L_n/\rho_i = 35$, $\eta_i = 3$, $k_y \rho_i = 0.1$, $T_i/T_e = 1$, $(k_z \rho_i)^{-1} = 3000$.

across the magnetic field, has a form

$$A + i\sqrt{\pi}W(z_{0i})B = 0, \quad (7)$$

where

$$\begin{aligned}
A &= (1 + iz_{0e}\sqrt{\pi}W(z_{0e})) (\tau z_{0i} + \chi_i) \\
&\times \left[(z_{0i} - \chi_i) (2A_{0i} - 1) - z_{0i}A_{0i} (S_i + \eta_i\chi_i z_{0i}) \right. \\
&\quad \left. + 2\eta_i\chi_i k_{\perp}^2 \rho_i^2 (A_{0i} - A_{1i}) \right] \\
&+ \left[1 + \tau (1 + i(z_{0e} - \chi_e)\sqrt{\pi}W(z_{0e})) \right. \\
&\quad \left. - A_{0i} (S_i + \eta_i\chi_i z_{0i}) \right] \\
&\times \left(\frac{k_{\perp}^2 \rho_i^2}{2\beta} + \frac{S_i A_{0i}}{2} - A_{0i} z_{0i} (z_{0i} Q_i - \chi_i) \right. \\
&\quad \left. + \eta_i \chi_i z_{0i} \left[A_{0i} z_{0i}^2 - k_{\perp}^2 \rho_i^2 (A_{0i} - A_{1i}) \right] \right) \\
&\quad + \left[A_{0i} (z_{0i} Q_i - \chi_i) \right. \\
&\quad \left. - \eta_i \chi_i z_{0i} \left[A_{0i} z_{0i}^2 - k_{\perp}^2 \rho_i^2 (A_{0i} - A_{1i}) \right] \right]^2 \quad (8)
\end{aligned}$$

and

$$\begin{aligned}
B &= \left(A_{0i} (z_{0i} Q_i - \chi_i) + \eta_i \chi_i \left[A_{0i} \left(\frac{1}{2} - z_{0i}^2 \right) \right. \right. \\
&\quad \left. \left. + k_{\perp}^2 \rho_i^2 (A_{0i} - A_{1i}) \right] \right) \\
&\times \left[\frac{k_{\perp}^2 \rho_i^2}{2\beta} + \frac{S_i A_{0i}}{2} - z_{0i} (z_{0i} - \chi_i) (1 - A_{0i}) \right. \\
&\quad \left. + \eta_i \chi_i z_{0i} k_{\perp}^2 \rho_i^2 (A_{0i} - A_{1i}) \right] = 0, \quad (9)
\end{aligned}$$

where $A_{0,1i} = I_{0,1}(k_{\perp}^2 \rho_i^2) e^{-k_{\perp}^2 \rho_i^2}$ and $Q_i = 1 - S_i$. In the case of the homogeneous ion temperature, i.e. for $\eta_i = 0$, Eq. (7) becomes identical to dispersion equation obtained and analysed in Ref.⁷. In this paper, the numerical analysis of Eq. (7) is performed with particular intent to ascertain the role of the ion temperature inhomogeneity on the DA instabilities in the presence of parallel sheared flow.

III. NUMERICAL SOLUTIONS AND DISCUSSIONS

In a general case, all terms in Eq. (7) are of the same order of value and the numerical analysis of Eq. (7) is necessary. The results of the numerical solution of Eq. (7) are presented in Figs. 1-7. In all these Figures (with the exception of Fig. 2) the results of the numerical solution for the normalized frequency ω/ω_{ci} are presented in panel (a), for the normalized growth rate γ/ω_{ci} in panel (b), for the parameter $|z_i|$ in panel (c), and for $|z_e|$ in panel (d). These solutions were derived for a plasma with $\beta = 5\%$ and $m_i/m_e = 1840$.

In Fig. 1, the solution to equation (7) is given versus L_n/ρ_i for $\eta_i = 3$, $k_y \rho_i = 0.1$, $T_i/T_e = 1$, $(V_0'/\omega_{ci})^{-1} = 70$, $(k_z \rho_i)^{-1} = 3000$. In this figure, as well as in all others, the plots for the kinetic Alfvén wave in a steady plasma are denoted by a green line (line 4), the plots for the DA

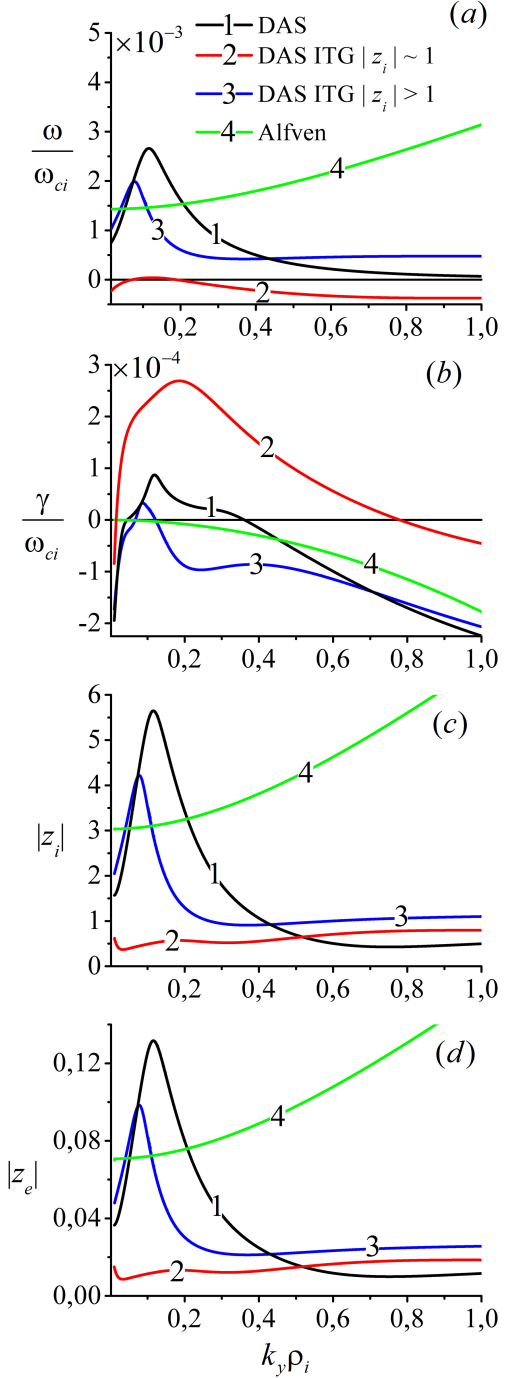


FIG. 5. The normalized frequency ω/ω_{ci} (panel (a)), normalized growth rate γ/ω_{ci} (panel (b)), $|z_i|$ (panel (c)) and $|z_e|$ (panel (d)) versus $k_y \rho_i$ for $L_n/\rho_i = 35$, $\eta_i = 3$, $(V_0'/\omega_{ci})^{-1} = 70$, $T_i/T_e = 1$, $(k_z \rho_i)^{-1} = 3000$.

instability in the shear flow (DAS instability) with homogeneous ion temperature (i. e. for $\eta_i = 0$) are denoted by a black line (line 1). It was found in Ref.⁷ that the solution to Eq. (7) for $\eta_i = 0$ reveals that the velocity shear is the factor which modifies the dispersion prop-

erties of the DA instability which develops⁸ in a steady plasma with cold ions ($T_i \ll T_e$) and is the source of the free energy for the development of other DAS instability which is absent in a steady plasma. It was derived⁷ that the left part of line 1 in Fig. 1 (panel (b)), which involves first localised maximum of the growth rate, corresponds to the shear-flow modified DAS instability. This instability develops as the DA instability due to the inverse electron Landau damping, however exists in the plasma with comparable inhomogeneous ion temperature. The right part of the line 1 with $L_n/\rho_i > 75$ corresponds to the shear flow driven DAS instability which develops due to the coupled action of the ion Landau damping and flow velocity shear. It was named in Ref.⁷ as the ion kinetic shear flow driven DAS instability. This instability has the growth rate larger than the growth rate of the modified DAS instability. It exists in the parallel sheared flow and is absent in the uniform plasma flow or steady plasmas. As it is presented in Figs. 1–7, these two DAS instabilities develop at different plasma parameters and at the different ranges of the wave number values.

The numerical solution to Eq. (7) with $\eta_i \neq 0$ predicts the development of two distinct DA instabilities in parallel sheared flow with inhomogeneous ion temperature (DAS-ITG instabilities). The plots for the frequency and the growth rate of the first DAS-ITG instability are denoted by a red line (line 2) and the plots for the second DAS-ITG instability are denoted by a blue line (line 3) in all Figs. 1 – 7. The panels (a), (b), (c) (d) of Figs. 1, 3–7 display that this instability develops under the conditions of the strong inverse ion Landau damping ($|z_i| \lesssim 1$) with the growth rate $\gamma(\mathbf{k})$ of the order of the frequency $\omega(\mathbf{k})$ and the useful estimate for the growth rate,

$$\gamma \sim k_z v_{Ti}, \quad (10)$$

follows. This instability may be named as the ion kinetic DAS-ITG instability.

The second DAS-ITG instability exists in the finite domain of the parameter L_n/ρ_i where the frequency of this instability and of the kinetic Alfvén wave are almost equal (Fig. 2 (panel b)) and where the ion Landau damping is weak (i. e. where $|z_i| \gg 1$ (Fig. 1 (panel (c))). This instability develops due to the inverse electron Landau damping with the growth rate (Fig. 1 (panel b)) much less than the frequency (panel (a)). It is the modified version of the DA instability of the steady plasmas⁸. In the parallel sheared flow, both DAS-ITG instabilities develop, as it follows from Fig. 7, in the plasma with cold as well as with hot ions where $T_i \gtrsim T_e$. The second DAS-ITG instability exists, however, only when the flow velocity shear is sufficiently strong (see Fig. 4 (panel (b))). Therefore this instability may be named as the electron kinetic shear flow modified DAS-ITG instability. As it follows from panel (b) of Fig. 2, the frequency of this instability in the parameters regions where the growth rate is maximum may be estimated as

$$\omega \sim k_y v_{de}. \quad (11)$$

Figure 1 displays that for the used values of the parameters the ion kinetic DAS-ITG instability develops for any values of L_n/ρ_i , whereas the electron kinetic shear flow modified DAS-ITG instability exists in the finite interval $20 \lesssim L_n/\rho_i \lesssim 80$. In Figs. 3 – 7, we use the value $L_n/\rho_i = 35$ for which both instabilities exist and both may be investigated.

In Fig. 3, the solution to equation (7) is given versus η_i for $L_n/\rho_i = 35$, $k_y \rho_i = 0.1$, $T_i/T_e = 1$, $(V'_0/\omega_{ci})^{-1} = 70$, $(k_z \rho_i)^{-1} = 3000$. This figure displays that the ion temperature inhomogeneity affects differently on these DAS-ITG instabilities. The growth rate of the electron kinetic sheared flow modified DAS-ITG instability gradually decay with parameter $\eta_i \sim L_n/L_{Ti}$ growth. At the same time, the ion temperature inhomogeneity has a decisive effect on the development of the ion kinetic DAS-ITG instability. This instability develops when parameter η_i becomes larger the threshold value with the growth rate growing with η_i value growth. Therefore, in fact only the ion kinetic DAS-ITG instability may be considered as a ion-temperature-gradient-driven instability. For $\eta_i = 3$ value, which is used in Figs. 1, 4–7, both DAS-ITG instabilities exist.

In Fig. 4, the solution to equation (7) is given versus $(V'_0/\omega_{ci})^{-1}$ for $L_n/\rho_i = 35$, $\eta_i = 3$, $k_y \rho_i = 0.1$, $T_i/T_e = 1$, $(k_z \rho_i)^{-1} = 3000$. Figure 4 displays, that the growth rates of both instabilities grow with growth of the flow velocity shearing rate. In the plasma with equal ion and electron temperatures, the electron kinetic shear flow modified DAS-ITG instability exists only in the limited range of the sufficiently large velocity shear. For the used numerical values of other parameters this instability exists only when $V'_0 > 10^{-2} \omega_{ci}$. The ion kinetic DAS-ITG instability continues to exist at any velocity shear values and stems from the coupled action of the flow velocity shear, ion temperature gradient and inverse ion Landau damping ($|z_i| \approx 1.2 \div 0.5$, $|z_e| \approx 10^{-2}$ (panels (c) and (d)). For $(V'_0/\omega_{ci})^{-1} = 70$ used in Figs. 1–7 (with the exception of Fig. 4) both DAS-ITG instabilities develop.

In Fig. 5, the solution to Eq. (7) is given versus $k_y \rho_i$ for $L_n/\rho_i = 35$, $\eta_i = 3$, $(V'_0/\omega_{ci})^{-1} = 70$, $T_i = T_e$, $(k_z \rho_i)^{-1} = 3000$. This figure reveals, that for the employed parameters the electron kinetic DAS-ITG instability develops in the narrow interval $\sim 0.05 \div 0.15$ of the $k_y \rho_i$ values with the growth rate much less than the frequency. At the same parameters, the ion kinetic DAS-ITG instability develops with the growth rate much above the frequency in the wide interval $\sim 0.05 \div 0.8$ of the $k_y \rho_i$ values. Note, that the frequency of the ion kinetic DAS-ITG instability changes its sign in this interval: it is positive in the narrow region of $k_y \rho_i$ where the growth rate is maximum being negative at the rest part of the $k_y \rho_i$ values. It follows from Fig. 5 that both DAS-ITG instabilities exist for the $k_y \rho_i = 0.1$ value used in the calculations presented in all other Figures.

In Fig. 6, the solution to Eq. (7) is given versus $(k_z \rho_i)^{-1}$ for $L_n/\rho_i = 35$, $\eta_i = 3$, $k_y \rho_i = 0.1$,

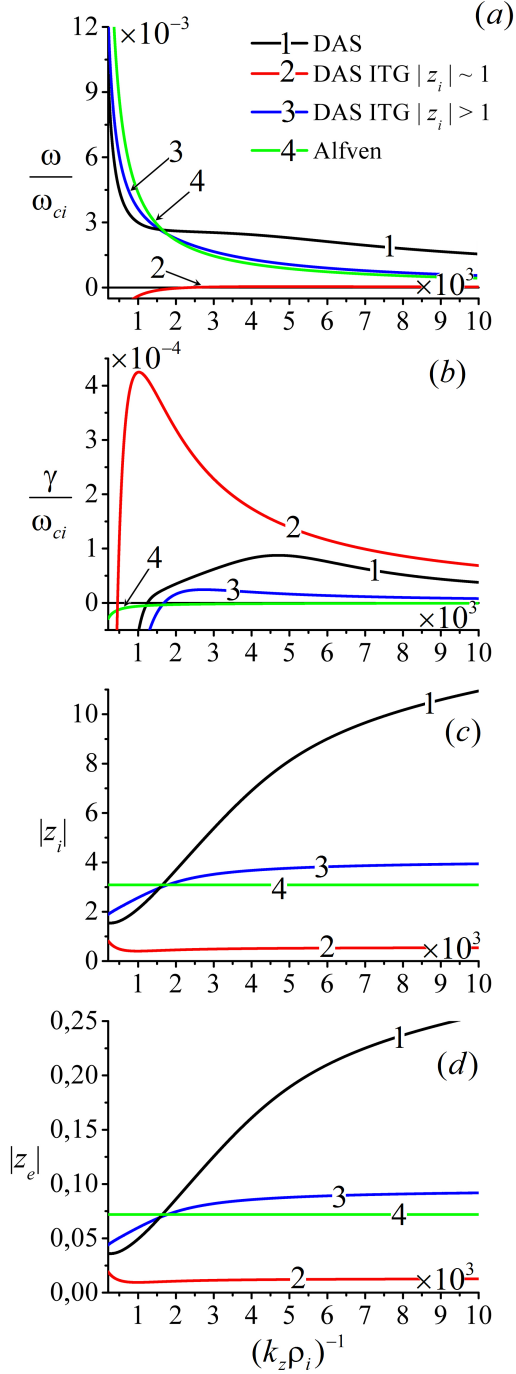


FIG. 6. The normalized frequency ω/ω_{ci} (panel (a)), the normalized growth rate γ/ω_{ci} (panel (b)), $|z_i|$ (panel (c)) and $|z_e|$ (panel (d)) versus $(k_z \rho_i)^{-1}$ for $L_n/\rho_i = 35$, $\eta_i = 3$, $k_y \rho_i = 0.1$, $(V'_0/\omega_{ci})^{-1} = 70$, $T_i/T_e = 1$ and $\beta = 5\%$.

$(V'_0/\omega_{ci})^{-1} = 70$, $T_i/T_e = 1$. The panel (b) displays that the ion kinetic DAS-ITG instability has largest growth rate in comparison with electron kinetic DAS-ITG instability and with DAS instability of a plasma with homogeneous ion temperature for all considered values of $(k_z \rho_i)^{-1}$. Moreover, the maximum growth rate of the ion

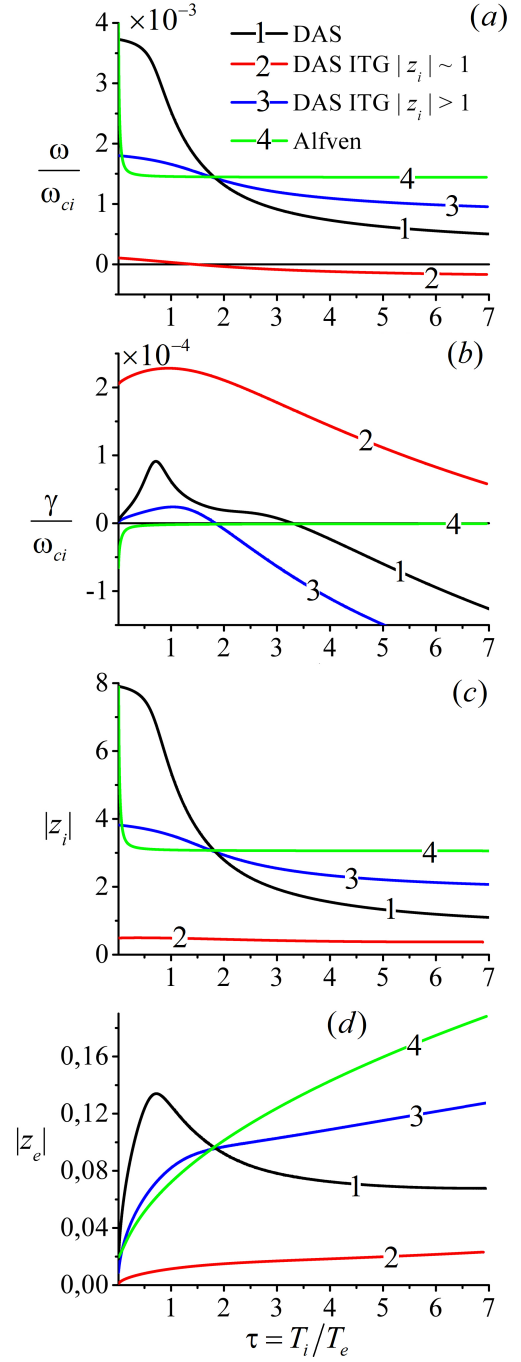


FIG. 7. The normalized frequency ω/ω_{ci} (panel (a)), the normalized growth rate γ/ω_{ci} (panel (b)), $|z_i|$ (panel (c)) and $|z_e|$ (panel (d)) versus $\tau = T_i/T_e$ for $L_n/\rho_i = 35$, $\eta_i = 3$, $k_y \rho_i = 0.1$, $(V'_0/\omega_{ci})^{-1} = 70$, $(k_z \rho_i)^{-1} = 3000$ and $\beta = 5\%$.

kinetic DAS-ITG instability attains for $(k_z \rho_i)^{-1}$ values ($(k_z \rho_i)^{-1} \lesssim 10^{-3}$) for which the electron kinetic DAS-ITG instability as well as the considered in Ref.⁷ DAS instabilities of the parallel sheared flow with homogeneous ion temperature are absent. In the calculations

presented in all other figures we used $(k_z \rho_i)^{-1} = 3000$ value for which both DAS-ITG instabilities exist and the ion kinetic instability has the growth rate approximately in two time less than the maximum value.

In Fig. 7, the solution to Eq. (7) is given versus T_i/T_e for $L_n/\rho_i = 35$, $\eta_i = 3$, $k_y \rho_i = 0.1$, $(V'_0/\omega_{ci})^{-1} = 70$, $(k_z \rho_i)^{-1} = 3000$. This figure displays that the DAS instability considered in Ref.7, and the electron and ion kinetic DAS-ITG instabilities develop in parallel sheared flow with warm ions. It is contrary to the steady plasmas where the DA instability may be developed only in plasma with $T_i \ll T_e$. The maximum growth rate attains for the plasma with $T_i \simeq T_e$ (DAS instability) or when $T_i \gtrsim T_e$ (both DAS-ITG instabilities). Panel (b) demonstrates that DAS instabilities and electron kinetic DAS-ITG instability exist in the finite ion/electron temperatures ratio interval which involves $T_i/T_e = 1$ value, used in all other Figures. The ion kinetic DAS-ITG instability exists for all considered values of the temperatures ratio.

IV. CONCLUSIONS

The numerical analysis of the dispersion equation (7), which accounts for the parallel flow shear, the inhomogeneous profiles of the plasma density and of the ion temperature, and the effects of thermal motion of ions was performed. It was derived, that the parallel sheared flow of a plasma with inhomogeneous ion temperature is unstable against the development of two distinct DAS-ITG instabilities. The performed numerical analysis of the dispersion equation (7) displays the existence of the shear flow driven ion kinetic DAS-ITG instability which develops due to the combined action of the flow velocity shear, ion temperature gradient and ion Landau damping. This instability has the growth rate of the order of the frequency. This growth rate is also much above the frequency of the electron kinetic DAS-ITG instability, which has the growth rate much less than the frequency.

Thus, the DA turbulence, which is powered by the DA instability existing only in a steady plasma with cold ions, $T_i \ll T_e$, relives in parallel sheared plasma flows with inhomogeneous ion temperature of the order of or above the electron temperature as DAS-ITG turbulence with much more larger growth rate. The initially fastest growing disturbance due to the ion kinetic DAS-ITG instability will dominate the subsequent development the DA turbulence in parallel shear flow. Certainly, because $\gamma(\mathbf{k}) \sim \omega(\mathbf{k})$ for this instability the nonlinear analysis of this instability with can't be performed on the base of the weak turbulence approach. Also, the renormalized nonlinear theory⁹, which accounts for the scattering of ions by the DAS turbulence, for which $\gamma(\mathbf{k}) \sim \omega(\mathbf{k})$ also⁹, may give analytically only the approximate estimate for the saturated amplitude of the electric field. The phase randomization of the waves in the wave packet with wave number spectrum width $\Delta k_\perp \sim k_\perp$ and the frequency

$\omega(\mathbf{k})$ occurs at time $t \sim \gamma^{-1}(\mathbf{k})$ when

$$\frac{d\omega(\mathbf{k})}{dk_\perp} \Delta k_\perp t \sim \frac{\omega(\mathbf{k})}{\gamma(\mathbf{k})} \gtrsim \pi, \quad (12)$$

but this does not occur for the ion kinetic DAS-ITG instability. There is no small parameter which can be applied for the development of any kind of the turbulence theory. The simplest estimates for the saturated amplitude of the electric field of the DAS-ITG turbulence powered by the considered DAS-ITG instabilities may be derived at the most general level by employing the widely invoked "mixing length estimate". It balances the wavelength of the perturbation against the particle (in our case the ion) displacement, ξ , in the unstable electric field,

$$\xi \sim \frac{u}{\gamma} \sim \frac{2\pi}{k_\perp}. \quad (13)$$

Eq. (13) defines the threshold for stochastization or mixing of a test ion trajectory and is the familiar for the instability saturation level¹⁰. With the estimates (10) for the growth rate $\gamma \sim k_z v_{Ti}$ and for the ion velocity $u \sim cE/B \sim ck_\perp \varphi/B$, Eq. (13) gives the estimate

$$\frac{e\varphi}{T_i} \sim \frac{k_z}{k_\perp} \frac{2\pi}{k_\perp \rho_i}. \quad (14)$$

This estimate is the same as was obtained in Ref.⁹ for the perturbed potential in the steady state of the ion kinetic shear flow driven DAS instability of a plasma with homogeneous ion temperature. Note, that the estimate (14) was obtained in Ref.⁹ employing the renormalized nonlinear theory, which accounts for the scattering of ions by the ensemble of DAS waves with random phases.

The mixing length estimate may be employed for the estimating the steady state level for the electron kinetic DAS-ITG instability. In this case the balance equation has a form

$$\xi \sim \frac{u}{\omega} \sim \frac{2\pi}{k_\perp}, \quad (15)$$

where the estimate for the frequency ω is given by Eq. (11). The estimate for the steady state level for the perturbed potential,

$$\frac{e\varphi}{T_i} \lesssim \frac{1}{k_\perp L_n}, \quad (16)$$

appeared to be the same as the obtained in Ref.⁹ for the electron kinetic shear flow modified DAS instability.

ACKNOWLEDGMENTS

This work was supported by National R&D Program through the National Research Foundation of Korea(NRF) funded by the Ministry of Education, Science and Technology (Grant No. NRF-2014M1A7A1A03029878) and BK21 Plus Creative Human Resource Development Program for IT Convergence.

DATA AVAILABILITY

The data that support the findings of this study are available from the corresponding author upon reasonable request.

- ¹N. Asakura, S. Sakurai, K. Itami, O. Naito, H. Tagenaga, S. Higashijima, Y. Koide, Y. Sakamoto, H. Kubo, and G. D. Porter, *J. Nucl. Mater.* **313**, 820 (2003).
- ²B. LaBombard, J. E. Rice, A. E. Hubbard, J. W. Hughes, M. Greenwald, J. Irby, Y. Lin, B. Lipschultz, E. S. Marmor, C. S. Pitchera, N. Smick, S. M. Wolfe, S. J. Wukitch and the Alcator Group, *Nucl. Fusion* **44**, 1047 (2004).
- ³N. Fedorczak, J. P. Gunn, Ph. Ghendrih, P. Monier-Garbet, A. Pocheau, *Journal of Nuclear Materials* **390–391**, 368 (2009).
- ⁴M. A. Pedrosa, C. Hidalgo, A. Lopez-Fraguas, M. A. Ochando, I. Pastor, E. Calderon and the TJ-II team, *Plasma Phys. Control. Fusion* **46**, 221 (2004).
- ⁵Guiding Wang, Long Wang, Xuanzong Yang, Chunhua Feng, Diming Jiang and Xiazhi Qi, *Plasma Phys. Control. Fusion* **40**, 429 (1998).
- ⁶V. V. Mikhailenko, V. S. Mikhailenko, Hae June Lee, M. E. Koepke, *Phys. Plasmas* **21**, 072117 (2014).
- ⁷V. V. Mikhailenko, V. S. Mikhailenko, Hae June Lee, *Phys. Plasmas* **23**, 020701 (2016).
- ⁸A. B. Mikhailovskii, *Electromagnetic Instabilities in an Inhomogeneous Plasma*. Institute of Physics Publishing, Bristol, 1992.
- ⁹V. V. Mikhailenko, V. S. Mikhailenko, Hae June Lee, *Phys. Plasmas* **23**, 092301 (2016).
- ¹⁰P. H. Diamond, S. I. Itoh, K. Itoh., *Modern Plasma Physics. Vol.1: Physical Kinetics of Turbulent Plasmas. Cambridge University Press, 2010*, p. 144.